




# Four-element MIMO antenna for X-band applications

[cambridge.org/mrf](https://www.cambridge.org/mrf)Ali Eslami , Javad Nourinia , Changiz Ghobadi and Majid Shokri 

Department of Electrical Engineering, Urmia University, Urmia, Iran

## Research Paper

**Cite this article:** Eslami A, Nourinia J, Ghobadi C, Shokri M (2021). Four-element MIMO antenna for X-band applications. *International Journal of Microwave and Wireless Technologies* **13**, 859–866. <https://doi.org/10.1017/S1759078720001440>

Received: 30 March 2020  
Revised: 23 September 2020  
Accepted: 25 September 2020  
First published online: 7 January 2021

### Keywords:

Circular polarization; MIMO antenna; X-band

### Author for correspondence:

Ali Eslami,  
E-mail: [st\\_a.eslami@urmia.ac.ir](mailto:st_a.eslami@urmia.ac.ir)

## Abstract

This study presents a new design of a four-element multiple-input multiple-output (MIMO) antenna, which is suitable for X-band applications. The circular polarization (CP) operation in this work is attained by using Tai Chi-shaped patches and L-shaped feeds. The proposed four-element MIMO antenna achieves two resonant frequencies, the first one at around 7.75 GHz and the second one with CP radiation is at approximately 10.15 GHz frequency. The measured isolations between ports with  $46.7 \times 46.7 \text{ mm}^2$  total dimensions are  $< -20 \text{ dB}$ . Due to the experiments, the envelope correlation coefficient for the orthogonal and parallel ports of the proposed MIMO antenna is  $< 0.003$  and  $0.005$ , respectively. Additionally, the presented antenna has a circularly polarized performance in the frequency band of 9.75–10.41 GHz and the average realized peak gain almost 2 dBic. The investigated antenna in this work is fabricated and tested in which the results are in a good agreement.

## Introduction

Multiple-input multiple-output (MIMO) technology uses array configuration by employing several antennas at two ends of the communication link. It is well-known that using MIMO antennas are inevitable for attaining high-speed data transmission and higher reliability [1]. On the other hand, improving the isolation characteristic of a MIMO system by consideration of device compactness is a significant challenge [2]. Till now, numerous MIMO antennas with different designs that use several isolation methods to improve the antenna performance were presented in the literature [3–8]. In [3, 4] two elements of the MIMO antennas are placed orthogonally to achieve isolation. In addition, to enhance the isolation, a parasitic structure embedded between elements in [4]. Furthermore, four-element MIMO antennas are presented in [5–8]. The antenna in [5] is comprised of a meander dipole, a reflector, and a parasitic strip. Four antenna elements in this design are located orthogonal to each other with a square loop configuration to reduce the size and improve the isolation. This antenna has an impedance bandwidth (IBW) of 23.9% (0.63, 2.32–2.95 GHz) while the isolations between the adjacent and opposite elements are  $< -14$  and  $-18 \text{ dB}$  with a total dimension of  $85 \times 85 \text{ mm}^2$ . Also, the envelope correlation coefficient (ECC) parameter between the adjacent and opposite elements is  $< 0.008$  and  $0.003$ , respectively. Another design of a four-element MIMO system, including L-monopole antennas, is reported in [6]. The mentioned antenna has IBW of 58.6% (2.24, 2.70–4.94 GHz), minimum isolation of 11 dB and ECC  $< 0.1$  with a total size of  $40 \times 40 \text{ mm}^2$ . In addition, a four-element MIMO antenna with half-circle shape monopoles is presented in [7], in which the antenna dimension is  $110 \times 60 \text{ mm}^2$  and 230 MHz IBW with minimum 11 dB isolation between the elements is realized. Most recently, a new four-element MIMO antenna composed of four symmetrical dipoles with integrated baluns is presented [8]. The parallel elements with the same polarization isolated from each other by choosing a suitable distance and the isolation of adjacent elements with orthogonal polarization are guaranteed by polarization diversity in this work.

Many other designs use more ports the same as the proposed antenna in [9], which presents an 8-element MIMO antenna.

Generally, MIMO antennas may have linear polarization (LP) or circular polarization (CP). However, typically the CP is preferred due to its advantages such as the ability to overcome multipath fading, admirable behavior in bad weather conditions, and acceptable mobility. Consequently, the CP produces a considerably high quality of communication service [10, 11]. Nowadays, many researchers attempt to design CP antennas with various techniques and satisfactory radiation properties [12–14]. One of these techniques is using Tai Chi-shape in antenna's configuration [15, 16]. In [15] by using an asymmetric microstrip feed line and a parasitic patch, a complete Tai chi-shape in the antenna structure is realized and it achieves IBWs from 3.1 to 4.58 and 4.97–6.53 GHz and axial ratio bandwidths (ARBW) from 3.26–4.42 and 5.45–6.63 GHz. In addition, a CP array antenna introduced in [16] uses semi-fractal radiation patches with Tai chi-shape, which covers the frequency range from 5.3 to 6.8 GHz and has ARBW from 5.4 to 6.6 GHz. The Tai Chi-shape for

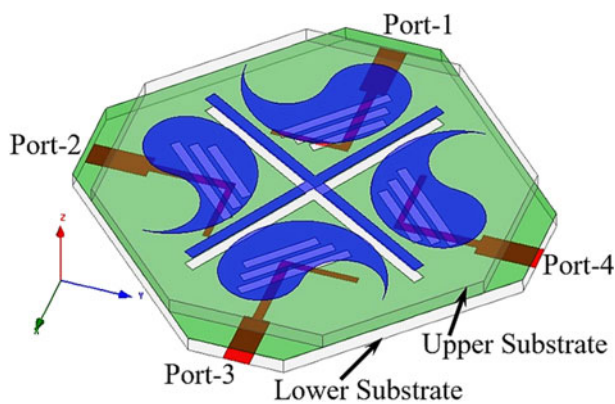


Fig. 1. The geometry of the proposed four-element MIMO antenna.

other purposes in antenna design such as radar cross-section (RCS) reduction is also used [17]. Furthermore, Tai Chi-shape element is used in [18] to realize a dual-band antenna covers two frequency bands from 2.4 to 2.49 GHz and from 5.07 to 5.88 GHz.

In this work, a new design of four-element MIMO antenna is presented which employed Tai Chi-shaped radiation elements and microstrip feed lines. The antenna achieves two resonant frequencies. The first one is at around 7.75 GHz and the second one with CP radiation is at approximately 10.15 GHz frequency. The measured isolations between ports with  $46.7 \times 46.7 \text{ mm}^2$  total dimensions are  $< -20 \text{ dB}$ . To realize the intended isolation, the adjacent feed lines are placed orthogonally to each other and decoupling crossed-slot and crossed-strip embedded to enhance the isolation. L-shaped feeds and appropriate rotation of surface currents on the Tai Chi-shaped patches generate the CP operation of the antenna. Because of the popular properties of printed patch antennas such as lightweight, acceptable radiation features and ease of fabrication, the proposed design is printed on FR4 substrates [19].

### Antenna design

The geometry of the proposed four-element MIMO antenna is shown in Fig. 1. The antenna comprises three conducting layers separated by two similar octagonal-shaped FR4 substrates with a thickness of 1.6 mm, loss tangent of 0.02, and permittivity of 4.4. As seen in this figure, the lower substrate contains four L-shaped microstrip feed lines at the four shorter edges and a ground plane. In this design, the feed lines and ground plane are located at the down and up sides of the substrate, respectively, in a way that the ground plane is common for all ports. Furthermore, three rectangular-shaped slots with different sizes are etched under each patch on the ground plane to generate an aperture-coupled structure. These slots approximately cover the patch surface above the L-shaped feed. In addition, the upper substrate, that only included four Tai Chi-shaped patches on the top side, is put over the lower substrate and fixed there. Accordingly, the thickness of the MIMO antenna becomes 3.2 mm.

It is worthwhile to mention that for accessing the ground plane and soldering the SMA connectors to the antenna ports, the upper substrate is truncated at the shorter edges by 2 mm. Accordingly, a Tai Chi-shaped patch, a microstrip line with L-shaped feed, three slots, and one port altogether produce one of the antennas of the MIMO system. The conductor layers of

the proposed antenna are illustrated in Fig. 2. As seen in Fig. 2 (a) the width and length of the microstrip lines to meet the  $50 \Omega$  impedance matching are chosen 2.7 and 6 mm, respectively, and connected to the L-shaped feeds to excite two orthogonal resonant modes for CP radiation. Moreover, the ground plane entitled middle conductor layer is shown in Fig. 2(b). It consists of three rectangular-shaped slots with lengths of 12, 10, and 8 mm and the width of 1 mm for each port to realize the aperture-coupled structure. To cover the majority of the patch surface by the feed, three slots between the patch and L-shaped feed are used. Thus, it produces approximately strong coupling. Besides, the Tai Chi-shaped patches are placed over the upper substrate as seen in Fig. 2(c). Moreover, decoupling crossed-strip between patches and decoupling crossed-slot etched on the ground plane between the ports is used to improve the isolation as shown in Fig. 2. According to this figure, the Tai Chi shapes are generated simply by a circle with a radius of  $R_p$  and two circles with a radius of  $R_p/2$ . The radius of  $R_p$  is set to 8.45 mm and the distance between antenna elements is fixed at 25 mm. Other dimensions are reported in Fig. 2. The radiation patch, slots, and feed line for each port are individual except the ground plane and decoupling elements, which are common for all ports.

### Results and discussion

The S-parameters of the MIMO antenna at four ports are depicted in Fig. 3.

Due to the symmetrical structure, the proposed antenna has similar responses for the ports, which indicate that two IBWs centered around 7.8 GHz and 10 GHz with  $S_{11} < -10 \text{ dB}$  are achieved. According to the simulated results, the MIMO antenna has IBWs of 7.72–7.99 GHz and 9.39–10.27 GHz for port-1, 7.69–7.98 and 9.38–10.26 GHz for port-2, 7.65–7.95 and 9.37–10.30 GHz for port-3, and 7.72–8.09 and 9.40–10.32 GHz for port-4. In addition, the isolation graphs of the proposed antenna between the different ports are reported in Fig. 4.

As seen in this figure, the isolations of more than 20 dB are realized for the proposed antenna. Two techniques are employed for improving the isolation in this work. First, the adjacent feeds are located orthogonally to each other and the second one, using decoupling structures between the radiating elements and similarly between the ground slots. Because of antenna compactness, we use a simple structure for decoupling. So a crossed-strip between patches and a crossed-slot on the ground plane between the ports is used to improve the isolation. In fact, the decoupling structures prevent the coupling currents from one port to another. The effect of the decoupling structures on the antenna isolations is illustrated in Fig. 5. Generally, the isolations can be separated into two categories in this design, isolation between the orthogonal ports and between the parallel ports.

Therefore, in this case, the ports, which are located in face-to-face positions, named parallel ports and the adjacent ports that are perpendicular to each other are called orthogonal ports. The figure clarifies that the presence of decoupling elements between the antenna ports improves the isolation significantly. Furthermore, a very important parameter in MIMO systems, which explains the coupling level between any two antennas, is the ECC. It is an appropriate manner to display the diversity performance of a MIMO system. Subsequently, smaller values for the ECC guarantees using reasonable antenna diversity. The ECC parameter can be evaluated from the S-parameters using (1) [20]. In this formula, the  $S(ii)$  is the reflection coefficient of

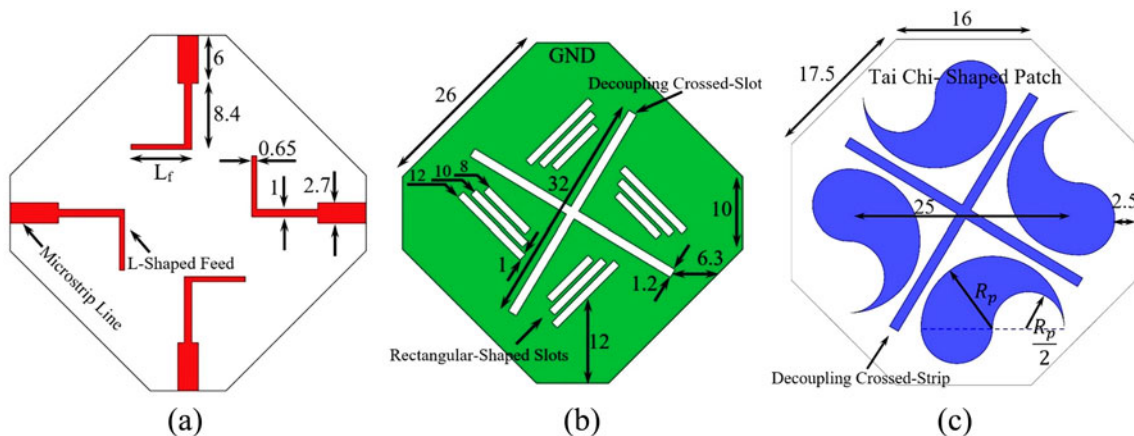


Fig. 2. Proposed four-element MIMO antenna: (a) bottom conductor layer, (b) middle conductor layer, and (c) top conductor layer. (All dimensions are in millimeter).

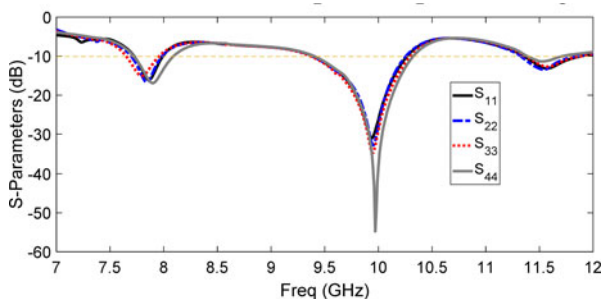


Fig. 3. Simulated S-parameters of the MIMO antenna for all ports.

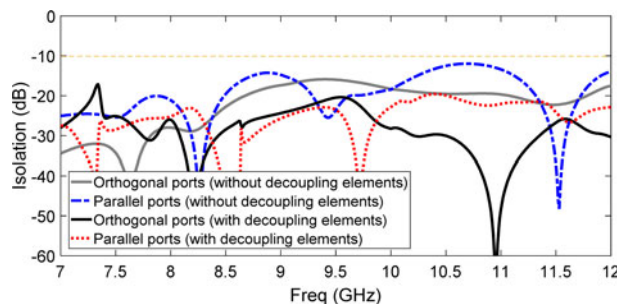


Fig. 5. The effect of the decoupling elements on the antenna isolations.

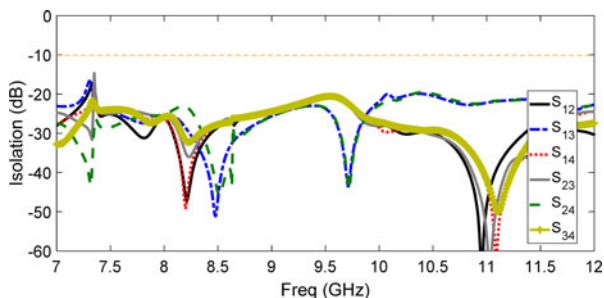


Fig. 4. Simulated isolations between the different ports of the MIMO antenna.

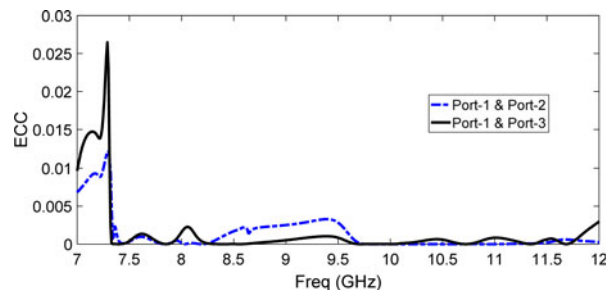


Fig. 6. ECC curves for the parallel and orthogonal ports of the proposed MIMO antenna system.

the antenna ( $i$ ) and  $S_{ij}$  (with  $i \neq j$ ), is the transmission coefficient between the antenna ( $i$ ) and the antenna ( $j$ ).

$$ECC = \rho_{ij} = \frac{|S_{ii}^* S_{ij} + S_{ji}^* S_{jj}|^2}{(1 - (|S_{ii}|^2 + |S_{ij}|^2))(1 - (|S_{jj}|^2 + |S_{ji}|^2))}. \quad (1)$$

Figure 6 exhibits the ECC curves for the parallel and orthogonal ports of the proposed MIMO antenna system with a maximum value of 0.005. Also, the figure shows that the correlation coefficient between the orthogonal ports is a little bit more than the parallel ports and the ECC almost equal to zero around the resonant frequencies.

On the other side, orthogonal electric fields are generated due to the feed and radiation patch shapes, which leads to exciting CP radiation. Indeed the Tai chi shape of patch provides good conditions to have a clock wise (CW) rotation for surface currents and improves the AR response of the MIMO antenna.

Figure 7 shows the simulated AR curves for the MIMO antenna at four ports. The 3-dB ARBW extends between 9.73 and 10.46 GHz for port-1, 9.72–10.42 GHz for port-2, 9.70–10.38 for port-3, and 9.74–10.46 for port-4 as presented in Fig. 7.

Moreover, the surface current distribution over the Tai Chi-shaped patch, at the frequency of lowest point of AR curve (10 GHz) is plotted in Fig. 8 whereas the port-1 is excited. As seen, it is clear that the surface currents with phases of  $0^\circ$ ,  $90^\circ$ ,



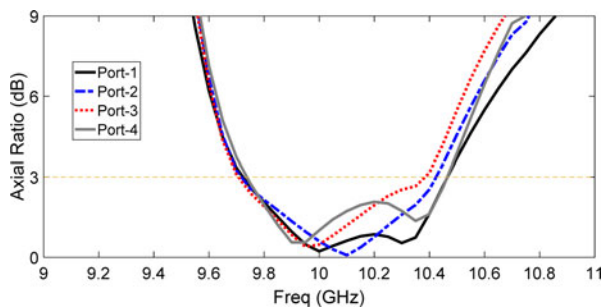


Fig. 7. Simulated AR curves for the MIMO antenna at port-1 to -4.

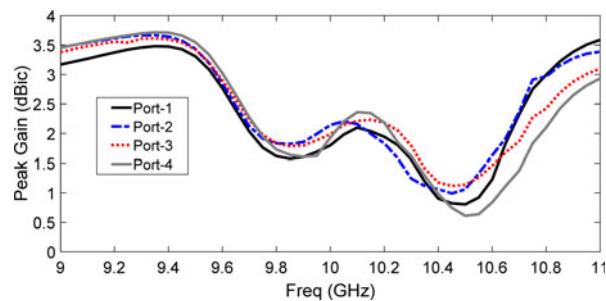


Fig. 9. Simulated gain curves for the MIMO antenna at port-1 to -4.

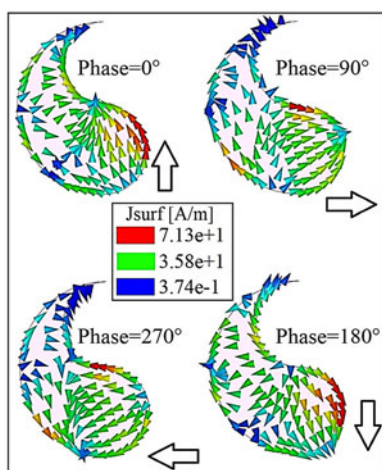


Fig. 8. Current distributions on the Tai Chi-shaped patch at 10 GHz in 0°, 90°, 180°, and 270° phases.

180°, and 270° have a CW rotation on the patch. In addition, the simulated gains for the proposed MIMO antenna with the optimized dimensions for four ports are shown in Fig. 9. The observed gains at all ports are almost equal and their variations are less than 2 dBic. The normalized right-hand CP (RHCP) and left-hand CP (LHCP) radiation patterns of the MIMO antenna at frequencies of 9.8, 10, and 10.2 GHz in the  $zy$ -plane ( $\varphi = 0^\circ$ ) are plotted in Fig. 10. All EM simulation results in this study have been carried out using high-frequency structure simulator (HFSS) Ver.13.

### Fabrication and measurements

The presented four-element MIMO antenna is fabricated by using two FR4 substrates and four SMA connectors. The fabricated structure is demonstrated in Fig. 11. The upper and middle conductor layers in Fig. 11(a), lower conductor layer in Fig. 11(b), and final structure of the proposed antenna in Fig. 11(c) are shown.

To measure the antenna's performance an Agilent network analyzer (E8363C) is used. The simulated and measured return loss responses for the proposed MIMO antenna at four ports are represented in Fig. 12 separately. Measured results indicate that the four-element MIMO antenna has IBWs of 7.58–8.04 GHz and 9.23–10.79 GHz for port-1, 7.56–8.12 GHz and 9.32–10.75 GHz for port-2, 7.48–7.96 GHz and 9.24–10.89 GHz for port-3, and 7.54–8.15 GHz and 9.28–10.61 GHz for port-4,

which is suitable for X-band applications. It has been proven that excellent isolation between the MIMO antenna elements improves the system performance.  $S_{ij}$  responses, where  $S_{ij}$  denotes the S-parameter for  $i$ th antenna and  $j$ th antennas, are a way to show how much the MIMO antenna elements are isolated from each other. Figure 13 displays the simulated and measured isolations of the four-element MIMO antenna between orthogonal ports (Fig. 13(a)), and parallel ports (Fig. 13(b)). Due to the measured results, the isolation between the elements in this work is better than  $-20$  dB.

Also, the simulated and measured ECC, peak gain, and ARBW of the proposed antenna are illustrated in Figs 14 and 15, respectively. The numerical and experimental results are in good agreement. According to the measured results, the ECC for orthogonal and parallel ports of the antenna is  $<0.003$  and  $0.005$ , respectively, in the operating frequency band. Furthermore, the proposed antenna has a wide ARBW from 9.75 to 10.41 GHz and the average realized peak gain of 2 dBic. As well, the simulated and measured normalized RHCP and LHCP radiation patterns of the proposed MIMO antenna at 10 GHz for port-1 are demonstrated in Fig. 16. According to the surface current distribution over the Tai Chi-shaped patch, at 10 GHz, it is clear that the surface currents with phases of 0°, 90°, 180°, and 270° have a CW rotation on the patch. So the RHCP is the dominant polarization of the antenna. This can be observed from the antenna radiation patterns. According to the patterns, it is shown that the RHCP radiation overcomes LHCP radiation. The simulated antenna efficiencies for the four ports of the MIMO antenna are presented in Fig. 17.

As shown in this figure, the simulated efficiencies at Port 1–4 are approximately 62% at 10 GHz frequency. The setup for radiation pattern measurement is shown in Fig. 18. In the measurement procedure, the port-1 is connected to an LG spectrum analyzer (SA-970) and the other ports are terminated with 50  $\Omega$  loads. The slight discrepancy between the simulated and measured results may be attributed to human errors and fabrication tolerances. Finally, to show the antenna advantages, two tables are given in this section. So, details of a fair comparison between the proposed four-element MIMO antenna and some recently similar designs are tabulated in Table 1. It is observed that the proposed antenna has two frequency band with a low correlation between the ports and compact size. Also, the proposed antenna has CP performance on the second frequency band, in a way that other designs do not have CP.

Moreover, the performance of the proposed antenna is compared with other designs, which employed Tai Chi-shaped structures in Table 2. According to this table, the proposed antenna exhibits a MIMO structure innovatively.

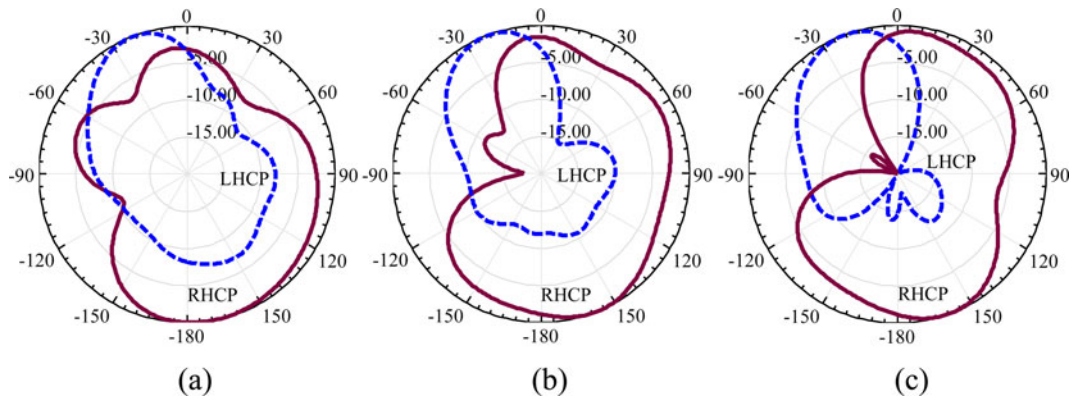


Fig. 10. Simulated normalized RHCP and LHCP radiation patterns of the MIMO antenna at frequencies of (a) 9.8, (b) 10, and (c) 10.2 GHz in the *zy*-plane (port-1).

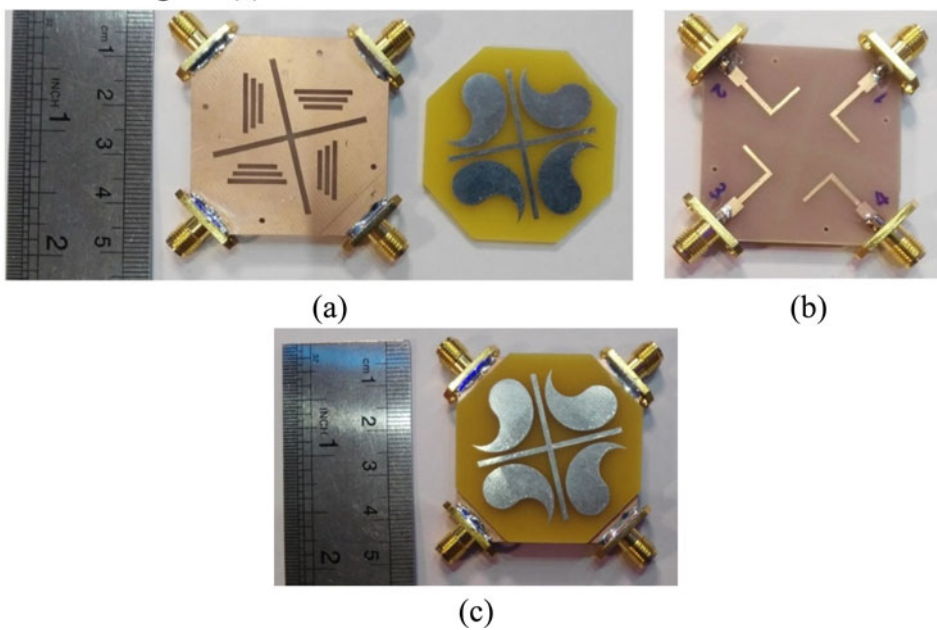


Fig. 11. Photographs of the fabricated antenna: (a) ground plane and Tai Chi-shaped patches, (b) antenna feed lines, and (c) final structure of the proposed four-element MIMO antenna.

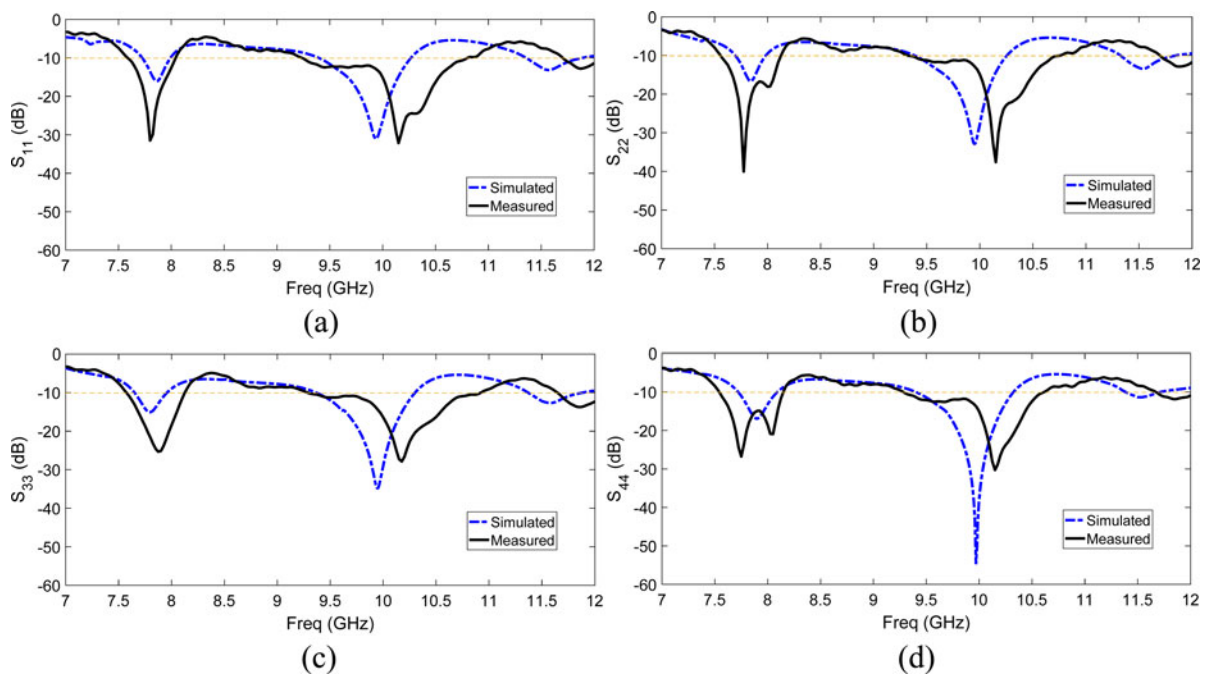


Fig. 12. Simulated and measured return loss responses for the proposed MIMO antenna, (a)  $S_{11}$ , (b)  $S_{22}$ , (c)  $S_{33}$ , and (d)  $S_{44}$ .

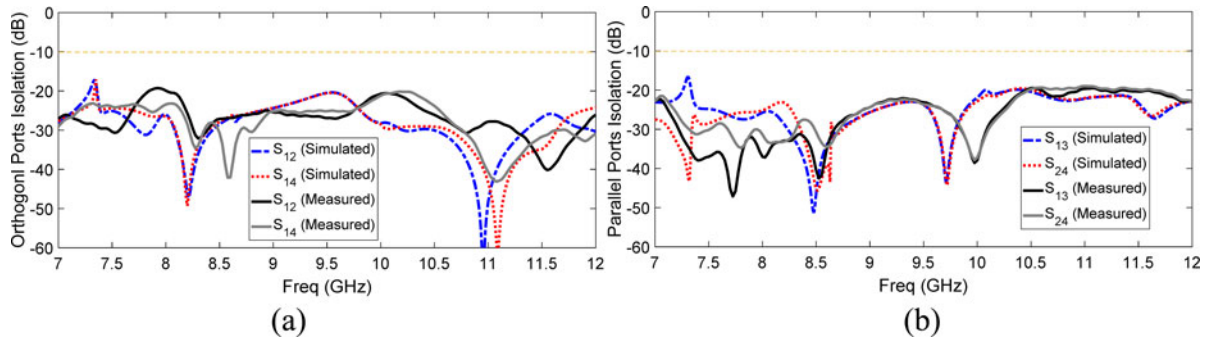


Fig. 13. Simulated and measured isolations between the proposed MIMO antenna ports: (a) orthogonal ports and (b) parallel ports.

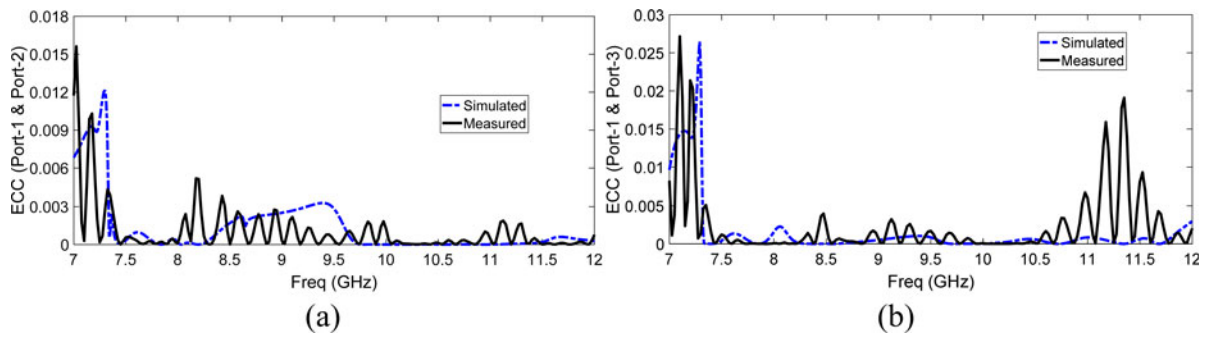


Fig. 14. Simulated and measured ECC between the proposed MIMO antenna ports: (a) orthogonal ports and (b) parallel ports.

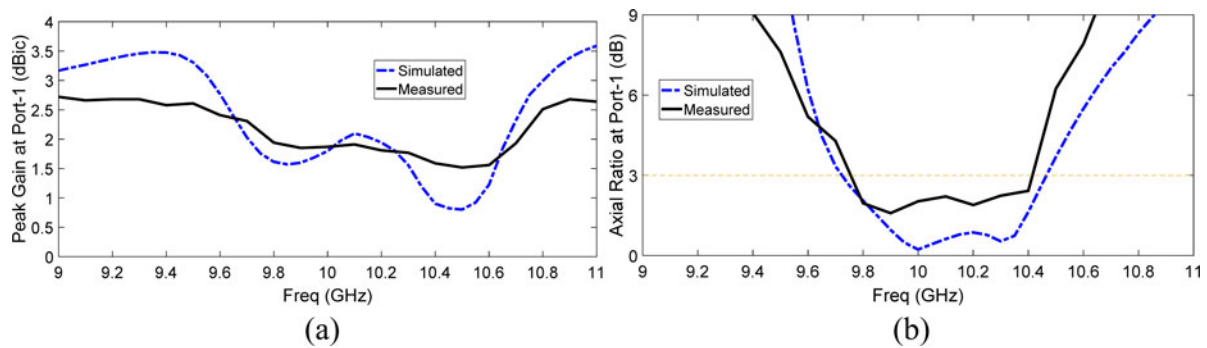


Fig. 15. Simulated and measured (a) peak gain and (b) ARBW of the proposed MIMO antenna for port-1.

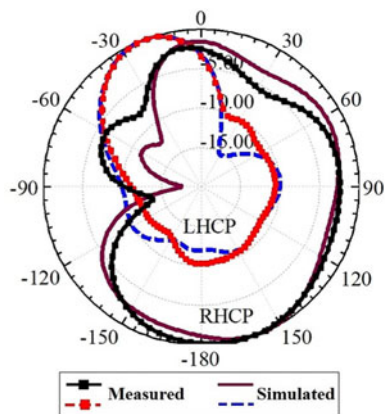


Fig. 16. Simulated and measured normalized radiation patterns of the proposed MIMO antenna at 10 GHz for port-1.

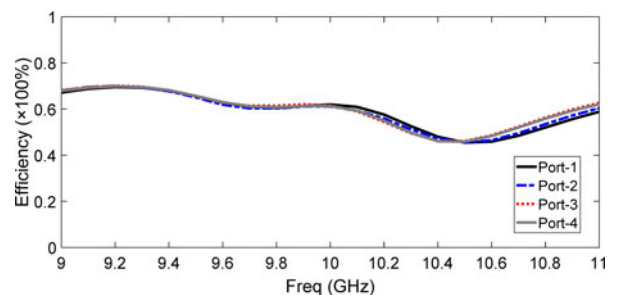


Fig. 17. Simulated antenna efficiencies at the four ports.



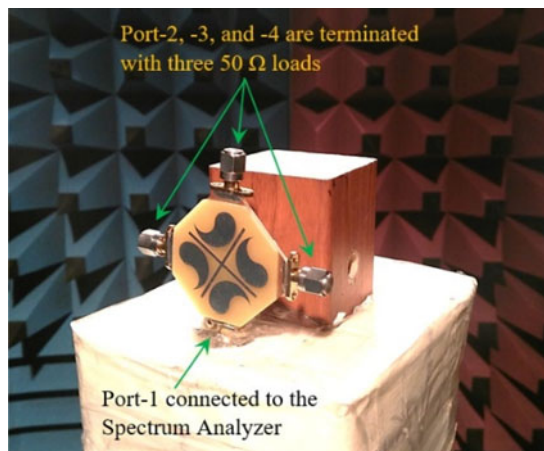


Fig. 18. Photograph of the proposed MIMO antenna in the RF anechoic chamber.

includes four Tai Chi-shaped patches on the top side, which is put over the lower substrate and fixed there. Moreover, three rectangular-shaped slots are etched under each patch on the ground plane to produce an aperture coupled structure. The rectangular-shaped slots cover the patch surface above the L-shaped feed. The proposed four-element MIMO antenna has two resonant frequencies, the first at around 7.75 GHz and the second one with CP radiation at about 10.15 GHz. The minimum measured isolations between antenna ports is at least 20 dB with  $46.7 \times 46.7 \text{ mm}^2$  total dimensions. Finally, the antenna is manufactured and tested with a good agreement between the simulations and measurements. The proposed design is suitable for X-band applications.

**Acknowledgement.** The authors would like to thank the Northwest Antenna and Microwave Research Laboratory (NAMRL) at Urmia University for technical supports.

Table 1. Comparison between the proposed four-element MIMO antenna and some similar recent designs.

Ref	IBW [GHz]	Isolation [dB]	Correlation coefficient	PG	Size $\text{mm}^2$	ARBW [GHz]	Substrate
[5]	23.9% (2.32–2.95)	$S_{12} \leq -17$ $S_{13} \leq -21$	$\text{ECC}_{12} < 0.008$ , $\text{ECC}_{13} < 0.003$	5.5 dBi	$85 \times 85$	–	Rogers 4003C
[6]	58.6% (2.70–4.94)	$\leq -11$	$\text{ECC} < 0.1$	4 dBi	$40 \times 40$	–	FR4
[7]	9.9% (2.2–2.43)	$\leq -11$	$\rho < 0.3$	3.12 dBi	$110 \times 60$	–	FR4
[8]	21.1 (2.20–2.72)	$\leq -15$	$\text{ECC} < 0.01$	8.37 dBi	$\pi \times 80^2$	–	FR4
This work	5.9% (7.58–8.04) & 15.6% (9.23–10.79)	$\leq -20$	$\text{ECC}_{12} < 0.003$ , $\text{ECC}_{13} < 0.005$	2.5 dBic	$46.7 \times 46.7$	6.5% (9.75–10.41)	FR4

P, correlation coefficient; ECC, envelop correlation coefficient; PG, realized peak gain; IBW, impedance bandwidth; ARBW, axial ratio bandwidths; MIMO, multiple-input multiple-output.

Table 2. Comparison between the proposed antenna with Tai Chi-shaped patches and some similar works which use Tai Chi-shaped structures.

Ref	IBW [GHz]	PG	Size $\text{mm}^2$	ARBW	MIMO configuration
[15]	37.3% (3.14–4.58) & 27.1% (4.97–6.53)	4.42 dBic, 4.15 dBic	$20 \times 16$	30.2% (3.26 to 4.42) 19.5% (5.45 to 6.63)	×
[16]	24.7% (5.37–6.89)	9.8 dBic	$20 \times 20$	20.4% (5.42–6.65)	×
[18]	3.7% (2.4–2.49 GHz) 14.8% (5.07–5.88 GHz)	1.75 dBi, 2.56 dBi	$15 \times 24$	–	×
This Work	5.9% (7.58–8.04) & 15.6% (9.23–10.79)	2.5 dBic	$46.7 \times 46.7$	6.5% (9.75–10.41)	4 × 4 MIMO Configuration

PG, realized peak gain; IBW, impedance bandwidth; ARBW, axial ratio bandwidths; MIMO, multiple-input multiple-output.

## Conclusion

A new design of circularly polarized MIMO antenna is investigated in this work. By employing Tai Chi-shaped patch with L-shaped feed, the CP performance is realized in this design. The proposed MIMO antenna in this study is composed of three conducting layers separated by two 1.6 mm-thickness FR4 substrates. The lower substrate comprises four L-shaped microstrip feed lines and a ground plane. Also, the upper substrate

## References

- Chen ZN, Liu D and Nakano H (2016) *Handbook of Antenna Technologies*. National University of Singapore, Singapore: Springer.
- Ren Z, Zhao A and Wu S (2019) MIMO Antenna with compact decoupled antenna pairs for 5G mobile terminals. *IEEE Antennas and Wireless Propagation Letters* **18**, 1367–1371.
- Aw M, Ashwath KRP and Ali T (2019) A compact two element MIMO antenna with improved isolation for wireless applications, *Journal of Instrumentation* **14**, P06014.

4. **Azarm B, Nourinia J, Ghobadi C and Majidzadeh M** (2019) Highly isolated dual band stop two-element UWB MIMO antenna topology for wireless communication applications. *Journal of Instrumentation* **14**, P10036.
5. **Ding K, Gao C, Qu D and Yin Q** (2017) Compact broadband MIMO antenna with parasitic strip. *IEEE Antennas and Wireless Propagation Letters* **16**, 2349–2353.
6. **Sarkar D and Srivastava KV** (2017) A compact four-element MIMO/diversity antenna with enhanced bandwidth. *IEEE Antennas and Wireless Propagation Letters* **16**, 2469–72.
7. **Hassan AT and Sharawi MS** (2016) Four element half circle shape printed mimo antenna. *Microwave and Optical Technology Letters* **58**, 2990–2992.
8. **Nasirzade R, Nourinia J, Ghobadi C, Shokri M and Naderali R** (2020) Broadband printed MIMO dipole antenna for 2.4 GHz WLAN applications. *Journal of Instrumentation* **15**, P01001.
9. **Zhao A and Ren Z** (2019) Size reduction of self-isolated MIMO antenna system for 5G mobile phone applications. *IEEE Antennas and Wireless Propagation Letters* **18**, 152–156.
10. **Mohammadi S, Nourinia J, Ghobadi C, Pourahmadazar J and Shokri M** (2013) Compact broadband circularly polarized slot antenna using two linked elliptical slots for C-band applications. *IEEE Antennas and Wireless Propagation Letters* **12**, 1094–1097.
11. **Shokri M, Rafii V, Karamzadeh S, Amiri Z and Virdee B** (2014) Miniaturised ultra-wideband circularly polarised antenna with modified ground plane. *Electronics Letters* **50**, 1786–1788.
12. **Shirzad H, Shokri M, Amiri Z, Asiaban S and Virdee B** (2013) Wideband circularly polarized square slot antenna with an annular patch. *Microwave and Optical Technology Letters* **56**, 229–33.
13. **Siahcheshm A, Nourinia J and Ghobadi C** (2018) Circularly polarized antenna array with a new sequential phase feed network utilizing directional coupler. *AEU - International Journal of Electronics and Communications* **93**, 75–82.
14. **Ellis M, Ahmed A, Kponyo J, Effah F, Nourinia J, Ghobadi C and Mohammadi B** (2019) Compact broadband circularly polarized printed antenna with a shifted monopole and modified ground plane. *Journal of Instrumentation* **14**, P11026.
15. **Saygin H, Rafiei V and Karamzadeh S** (2018) A new compact dual band CP antenna design. *Microwave and Optical Technology Letters* **60**, 594–600.
16. **Karamzadeh S, Saygin H and Rafiei V** (2018) Circularly polarized array antenna with emphasis on the reduction of RCS by utilizing semi-fractal elements. *2018 International Conference on Communications (COMM)*.
17. **Luo X, Zhang Q and Zhuang Y** (2017) Tai-Chi-Inspired pancharatnam-berry phase metasurface for dual-band RCS reduction. *2017 IEEE International Symposium on Antennas and Propagation & USNC/URSI National Radio Science Meeting*.
18. **Niu X, Liang J, Wu G-C and Lin Y** (2016) Compact dual-band ACS-fed monopole omnidirectional antenna for 2.4/5.2/5.8 GHz WLAN applications. *Frequenz* **70**, 211–218.
19. **Shokri M, Rafii V, Karamzadeh S, Amiri Z and Virdee B** (2016) CPW-fed printed UWB antenna with open-loop inverted triangular-shaped slot for WLAN band filtering. *International Journal of Microwave and Wireless Technologies*, **8**, 257–262.
20. **Li J, Zhang X, Wang Z, Chen X, Chen J, Li Y and Zhang A** (2019) Dual-band eight-antenna array design for MIMO applications in 5G mobile terminals. *IEEE Access* **7**, 71636–71644.



antennas, and antenna's polarization species.

**Ali Eslami** was born in Zanjan, Iran in 1991. He received his B.Sc. in Information and Communication Technology Engineering from Roozbeh Institute of Higher Education, Zanjan, Iran in 2013 and M.Sc. degree in Electrical – Telecommunications from Urmia University, Urmia, Iran in 2019. Since 2019, he is researching on antenna species and his areas of interest are antenna design, microstrip



is a professor in the Department of Electrical Engineering of Urmia University, Urmia, Iran. His primary research interests are in antenna design, numerical methods in electromagnetic, and microwave circuits.

**Javad Nourinia** received his B.Sc. in Electrical and Electronic Engineering from Shiraz University and M.Sc. degree in Electrical and Telecommunication Engineering from Iran University of Science and Technology, and Ph.D. degree in Electrical and Telecommunication from University of Science and Technology, Tehran, Iran in 2000. From 2000 he was an assistant professor and now he



Electrical Engineering of Urmia University, Urmia, Iran. His primary research interests are in antenna design, radar and adaptive filters.

**Changiz Ghobadi** was born in Iran on June 1, 1960. He received his B.Sc. in Electrical Engineering-Electronics and M.Sc. degrees in Electrical Engineering from Isfahan University of Technology, Isfahan, Iran and Ph.D. degree in Electrical- Telecommunication from University of Bath, Bath, the UK in 1998. From 1998 he was an assistant professor and now he is a professor in the Department of



polarized antennas and microwave circuits.

**Majid Shokri** was born in Urmia, Iran in 1979. He received the B.Sc. and M.Sc. degrees from the Urmia Branch, IAU and Urmia University in 2001 and 2012, respectively, both in electrical and communication engineering. Since 2018 he is pursuing the Ph.D. degree in communication engineering with the Department of Electrical Engineering, Urmia University. His areas of interest are microstrip antennas, circularly